Self-normalized photothermal technique for accurate thermal diffusivity measurements in thin metal layers

J. A. Balderas-López[a] and A. Mandelis
Center for Advanced Diffusion-Wave Technologies (CADIFT), Department of Mechanical and Industrial Engineering, University of Toronto, 5 King's College Road, Toronto, Ontario M5R 3G8, Canada

A self-normalized photothermal method for measuring thermal diffusivity of thin metal layers has been implemented using two experimental configurations based on photothermal radiometry and gas-cell photoacoustic detection. The corresponding measurement procedures involve linear fits in the photothermally thin and/or thick limits. As part of this method, simple experimental criteria have been developed to ascertain that a purely thermal-diffusion-wave mechanism is dominant throughout the selected frequency range, thus validating the accuracy of the thermal diffusivity measurements. Thermal-diffusivity values measured using the intrinsic reliability of this self-normalized photothermal measurement scheme are reported for two commercial samples of aluminum and steel thin layers. © *2003 American Institute of Physics.*
[DOI: 10.1063/1.1623626]

I. INTRODUCTION

Frequency-domain photothermal (PT) techniques have been used extensively for thermal and optical diagnostics of many types of materials.[1–6] The general principle behind these techniques involves absorption of modulated radiation. The fraction of absorbed radiation, which is transformed into heat, increases the temperature of the material. PT signals generated from the subsequent heat diffusion (thermal wave) and/or radiation transport mechanisms provide information about the optical and thermal properties of the material. A major application of PT techniques lies in the area of thermal diffusivity measurements of solids.[2–7] Generally speaking, the corresponding measurement methodologies involve the analysis of the PT signal as a function of the modulation frequency. Photoacoustic spectrometry and infrared photothermal radiometry (PTR) are two popular PT detection methodologies. The analysis of PT signals in the frequency domain, however, may be complicated because they are convoluted with the transfer function of the measurement system electronics. A very convenient way to eliminate the transfer function is by an appropriate normalization procedure. The use of data normalization is such a procedure, because, aside from the elimination of the transfer function, it reduces the number of parameters required for quantitative analysis, thus increasing simplicity and reliability.[5–7] Although the application of PT techniques to metals involves a relatively simple model based on surface optical absorption, data analysis faces some difficulties, even though the transfer function is eliminated. At low modulation frequencies, three-dimensional (3D) effects may appear mainly due to the generally long thermal-diffusion length in some metals owing to

their high thermal diffusivity. At high modulation frequencies, the weak photoacoustic signal is highly influenced by other phenomena, such as thermoelastic contributions.

In this article, a self-normalization procedure is developed for measuring the thermal diffusivity of metals using two PT methodologies: photoacoustic (PA) and radiometric detection. The new method is based on the signal ratio for front and rear surface experimental configurations[7] and develops a set of reliability criteria verifying detection of purely thermal-diffusion-wave-generated PT signals within the entirely thermally thin or thermally thick limit.[8] Starting with raw normalized data (no instrumental transfer function correction is involved), the rigorous application of the relevant theory resulting from the one-dimensional diffusion-wave problem is used to build the necessary experimental criteria for reliable measurements of the thermal diffusivity of metals. Two of these criteria involve normalized signals in the thermally thin limit (low modulation frequencies) and the thermally thick limit (high modulation frequencies), respectively. At low modulation frequencies, the analytical procedure is based on the linear behavior between the tangent of the normalized phase difference between the rear and the front PT configurations and modulation frequency. In the thermally thick limit, the analysis is based on the linear behavior of the phase difference with the square root of the modulation frequency. Unlike earlier self-normalized PT methods,[3,7] the criteria developed in the present technique allow for direct comparison with theoretical predictions within the purely thermal-diffusion-wave limits, thus clearly identifying and avoiding frequency ranges where the superposition of complicating mechanisms, such as thermoelastic PA behavior, contribute or even dominate. Upon application of the developed criteria, further simplification of signal interpretation and diffusivity measurements occurs since the data analysis is carried out in the entirely thermally thin and thick limits. Overall, the developed criteria improve the reli-

---
[a]Also at: Unidad Profesional Interdisciplinaria de Biotecnología del IPN, Av. Acueducto S/N, Col. Barrio la Laguna, Del. Gustavo A. Madero, C. P. 07340, México, D. F., México;
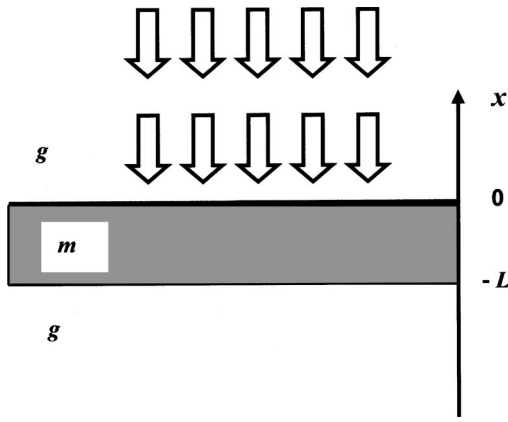electronic mail: abalderas@acei.upibi.ipn.mx

5219

FIG. 1. Schematic of the 1D single-layer photoacoustic model with surface absorption. g: gas (air) and m: metal sample.

ability of the quantitative analysis over published PA methodologies in which the domination of the thermal-diffusion-wave mechanism is assumed to be valid *a priori*,[7] or the frequency range is selected by assuming specific modulation frequency dependencies.[3]

II. THEORETICAL CONSIDERATIONS

A one-dimensional (1D) PT geometry is depicted in Fig. 1. A single layer of the optically opaque material m, is embedded in, or surrounded by, a transparent medium g. Optical radiation, e.g., from a laser source, of intensity I_0 and angular modulation frequency $\omega = 2\pi f$, impinges on the upper surface of m, which absorbs light on its surface, modeled as a very thin layer with an optical absorption coefficient β. The corresponding differential equations for 1D heat diffusion are

$$\frac{\partial^2 T_g}{\partial x^2} - \frac{1}{\alpha_g}\frac{\partial T_g}{\partial t} = 0 \quad 0 \leq x$$

$$\frac{\partial^2 T_m}{\partial x^2} - \frac{1}{\alpha_m}\frac{\partial T_m}{\partial t} = -\frac{\beta I_0 \delta(x)}{2 k_m}[1 + e^{i\omega t}], \quad -L \leq x \leq 0,$$

(1)

$$\frac{\partial^2 T_g}{\partial x^2} - \frac{1}{\alpha_g}\frac{\partial T_g}{\partial t} = 0 \quad -\infty < x \leq -L,$$

with boundary conditions

$$T_g(0) = T_m(0)$$

$$T_m(-L) = T_g(-L)$$

$$-k_m \frac{dT_m}{dx}\bigg|_{x=0} = -k_g \frac{dT_g}{dx}\bigg|_{x=0} + HT_m(0)$$

$$-k_m \frac{dT_m}{dx}\bigg|_{x=-L} = -k_g \frac{dT_g}{dx}\bigg|_{x=-L} - HT_m(-L)$$

and the physical requirement of finite solutions as $x \to \pm\infty$:

$$\lim T_g(x) = 0,$$

$$x \to \pm\infty.$$

Here, T_i, $i = g, m$, is the temperature distribution inside medium i, k_m is the thermal conductivity of medium m and H, defined as $H = 4\epsilon\sigma T_\theta^3 (\mathrm{W\,m^{-2}\,K^{-1}})$, is a radiometric heat transfer coefficient through infrared emissions, ϵ is the surface emissivity, and $\sigma = 5.67 \times 10^{-12}\,\mathrm{W/cm^2\,K^4}$ is the Stefan–Boltzmann constant.

Solution of the coupled differential equations shows that the harmonically modulated front (F) and rear (R) surface temperature is given by

$$T_F(f) = \frac{\beta d I_0}{k_s \sigma_s}\left[\frac{(1 + b_{gs} + h)e^{\sigma_s L} + (1 - b_{gs} - h)e^{-\sigma_s L}}{(1 + b_{gs} + h)^2 e^{\sigma_s L} - (1 - b_{gs} - h)^2 e^{-\sigma_s L}}\right]$$

at $x = 0$, (2)

$$T_R(f) = \frac{\beta d I_0}{k_s \sigma_s}\left[\frac{2}{(1 + b_{gs} + h)^2 e^{\sigma_s L} - (1 - b_{gs} - h)^2 e^{-\sigma_s L}}\right]$$

at $x = -L$. (3)

In these two equations, σ_k, $k = g, m$ is the complex thermal diffusion coefficient of medium k, (βd) is the surface absorptance of medium m, $b_{gs} = e_g/e_s$, is a ratio of thermal effusivities and $h = H/k_s \sigma_s$. According to the Rosencwaig–Gersho theory[8] of the gas-cell PA effect and similar models for the infrared radiometric (PTR) signal,[9] both signals are proportional to the temperature fluctuations of the sample surface. Taking the ratio $R(f) = T_R(f)/T_F(f)$, it is clear that several common terms on Eqs. (2) and (3) are eliminated, and so is the instrumental transfer function. As a result, the following simple expression is obtained:

$$R(f) = \frac{2}{(1 + b_{gs} + h)e^{\sigma_s L} + (1 - b_{gs} - h)e^{-\sigma_s L}}.$$

(4)

Considering that for metals b_{gs} is approximately equal to zero and, for typical modulation frequency ranges, $h \approx 0$,[10] the amplitude $|R|$ and phase Φ of the complex signal $R(f)$ can be written as[7]

$$|R| = \frac{\sqrt{2}}{(\cosh(2x) + \cos(2x))^{1/2}},$$

(5)

$$\tan(\Delta\Phi) = -\tanh(x)\tan(x),$$

(6)

where $x = (\pi f/\alpha_m)^{1/2}L$. In principle, both of these equations can be used for thermal diffusivity measurement purposes in metals, however, as was pointed out before, the lack of appropriate modulation frequency-range selection criteria for a purely thermal-diffusion-wave mechanism may complicate the analysis. This is especially true for the PT amplitude ratio [Eq. (4)], which is highly sensitive to light source fluctuations, surface reflectivity, or differences on laser beam intensities. Equations (2)–(6) were derived assuming identical surface and laser beam properties on both sides of our materials. In practice, however, variations may cause departures from the strict validity of the foregoing thermal-wave equations, which will require corrections to yield accurate thermal diffusivity measurements. The phase difference $\Delta\Phi$ is more suitable for these measurements than the amplitude ratio $|R|$, because the former is independent of surface optical

TABLE I. Thermal diffusivity values of thin aluminum and steel samples, obtained by the two PT methodologies reported in this article. $\alpha_{\text{Thin}}^{\text{PA}}$ and $\alpha_{\text{Thick}}^{\text{PA}}$ stand for the PA thermal diffusivity measurements in the thermally thin and thermally thick limit, respectively. $\alpha_{\text{Thin}}^{\text{PTR}}$ and $\alpha_{\text{Thick}}^{\text{PTR}}$ are similar measurements using the PTR technique.

Material	Thickness (cm)	$\alpha_{\text{Thin}}^{\text{PA}}$ (cm²/s)	$\alpha_{\text{Thick}}^{\text{PA}}$ (cm²/s)	$\alpha_{\text{Thin}}^{\text{PTR}}$ (cm²/s)	$\alpha_{\text{Thick}}^{\text{PTR}}$ (cm²/s)
Aluminum (commercial)	0.0300 ±0.0005	0.34 ±0.01	0.38 ±0.03	0.38 ±0.04	0.59 ±0.08
Steel sample	0.0560 ±0.0005	0.100 ±0.003	0.110 ±0.010	0.120 ±0.004	0.120 ±0.008

factors and laser intensity. Moreover, it is possible to derive simpler expressions for $\Delta\Phi$ and $\tan(\Delta\Phi)$ at high and low modulation frequencies. At low frequencies, this can be done by considering a Taylor series expansion for the functions $\tanh(x)$ and $\tan(x)$[10,11]:

$$\tanh(x) \approx x - x^3/3 + 2x^5/15 - \ldots$$

and

$$\tan(x) \approx x + x^3/3 + 2x^5/15 + \ldots$$

Upon keeping only linear terms in the thermally thin limit of $x \ll 1$, it can be easily shown that

$$\tan(\Delta\Phi) \approx -x^2 = -\left[\frac{\pi}{\alpha_m}L^2\right]f. \tag{7}$$

The next term in the series expansion for $\tan(\Delta\Phi)$ involves $O(x^6)$, so the approximation given by Eq. (7) is very accurate for $x < 0.6$. For example, given typical values $\alpha_m = 0.98$ cm²/s and $L = 0.03$ cm for aluminum foils, a modulation frequency of $f = 100$ Hz, yields $x = 0.53$, $x^2 = 0.28$, and $x^6 = 0.022$. Equation (7) shows that a linear relation of $\tan(\Delta\Phi)$ with f is expected in the thermally thin limit. In this limit, the sample thermal diffusivity can be easily obtained from the slope/fitting parameter $M = (\pi/\alpha_m)L^2$.

In the thermally thick limit, the asymptotic behavior for $\Delta\Phi$ can be considered instead. From Eq. (6), it is easy to show that if $x \gg 1$, then

$$\Delta\Phi \approx -x = -\left(\sqrt{\frac{\pi}{\alpha_m}}L\right)\sqrt{f}. \tag{8}$$

This equation shows that the phase $\Delta\Phi$ behaves asymptotically as $f^{1/2}$. The corresponding analytical procedure based on Eq. (8) involves the fitting of the experimental phase difference $\Delta\Phi$ as a function of the square root of the modulation frequency in the range of high modulation frequencies. In the thermally thick limit, the sample thermal diffusivity can be obtained from the slope/fitting parameter $P = (\pi/\alpha_m)^{1/2}L$.

In view of the fact that Eq. (6) is independent of instrumental factors, the predicted requirements that $\tan(\Delta\Phi) \to 0$ and $\Delta\Phi \to 0$ for $f \to 0$, must be rigorously applied and constitutes additional criteria for selecting the appropriate frequency range for quantitative measurements in the thermally thin or thick limits, respectively. An additional criterion can be obtained from Eq. (5) which predicts a flat behavior for the ratio of amplitudes at very low modulation frequencies where $x \ll 1$. The foregoing criteria are useful for testing the validity of the 1D analysis in the range of very low modulation frequencies, where 3D PT effects may be present, or in the range of high modulation frequencies, where deviations from the purely diffusion-wave mechanism (e.g., with the PA probe), combined with poor signal-to-noise ratios (SNRs), could compromise the reliability and precision of the measurement.

III. EXPERIMENTAL CONFIGURATIONS

Two metal samples were used in this work (Table I): A commercial aluminum slab (originally 4 mm thick) and a steel foil (560 μm thickness). A small piece of the aluminum sample was cut and polished to obtain a thin layer of 300 μm thickness, as measured with the help of a micrometer calibrator (Mitutoyo, ±5 μm precision). Similarly, a 560 μm piece of steel (unknown composition) was used.

A. Photoacoustic setup

The experimental gas-cell PA setup, shown in Fig. 2, consisted of an argon-ion laser (approximately 1 mm beam diameter), delivering 200 mW of dc power, the beam of which was modulated by means of an acousto-optic modulator. The PA cell consisted of a cylindrical hole (3 mm diameter and 3 mm height), made in a brass body and communicating with
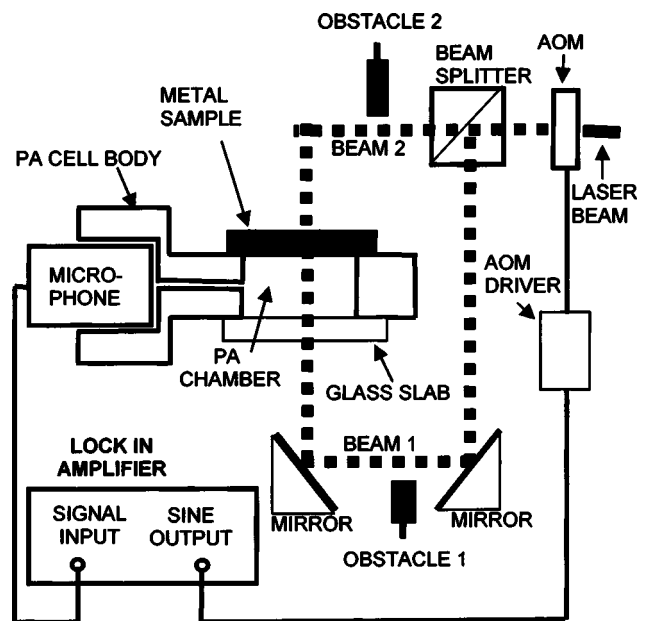
FIG. 2. Experimental PA setup used for the implementation of the self-normalized procedures. AOM: acousto-optic modulator.
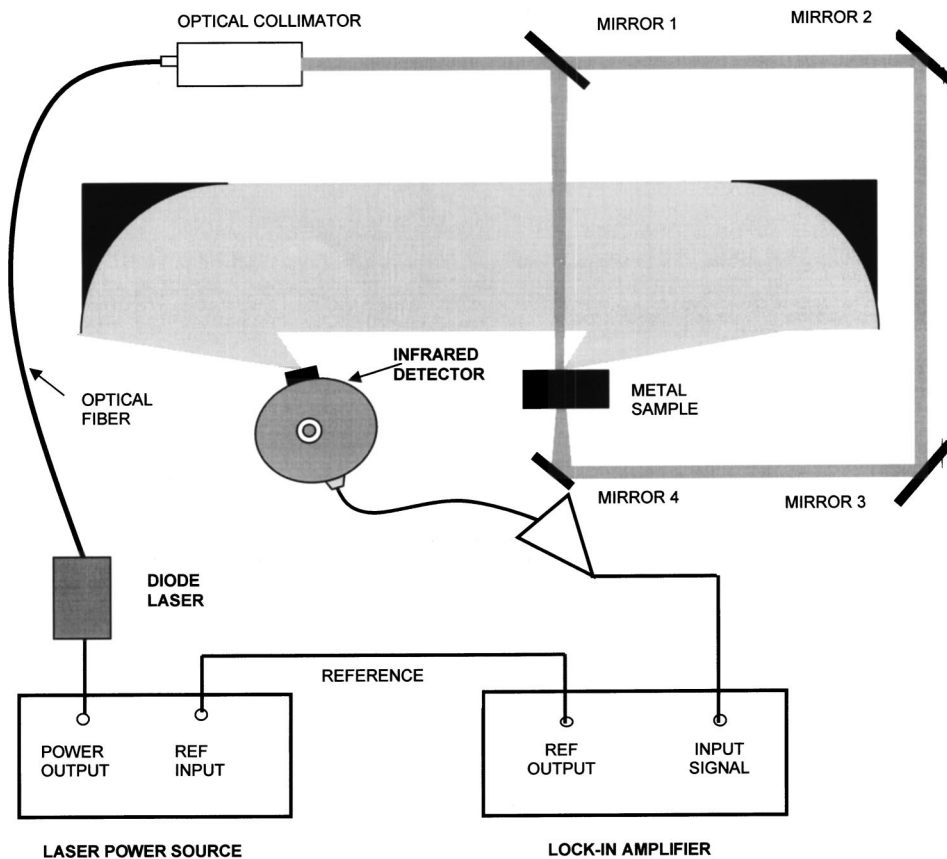
FIG. 3. Experimental infrared PT radiometric setup used for the implementation of the self-normalized method.

an electret microphone (with a built-in preamplifier) through a channel. The PA chamber was obtained by placing the metallic sample on the upper surface of the cell using vacuum grease. It was sealed by using a thin 160 μm plate of Corning glass on the opposite side, which also served as an optical window. To obtain the front and rear PA configurations, the modulated laser beam was first directed to a beamsplitter, Fig. 2. The PA signal for the rear configuration was obtained by allowing only beam 2 in Fig. 2 to impinge on the upper surface of the sample. This was achieved by obstructing beam 1. The PA signal for the front configuration was obtained by reversing the roles of beams 1 and 2. PA signals for both configurations were generated in a range of 3 to 501 Hz, for the aluminum sample and 3 to 151 Hz for the steel sample using a step of 2 Hz. The signals were fed to a lock-in amplifier (SRS, Model 830) for further amplification and demodulation.

B. Radiometric setup

The experimental infrared photothermal radiometric setup, shown in Fig. 3, consisted of an infrared diode laser ($\lambda=830$ nm) with a fiber-optic pigtail (Opto-Power Corp.) collimated to ~0.5 mm beam diameter, delivering 400 mW of continuous-wave power. Intensity modulation of the laser light was achieved through current modulation of the diode (power supply Coherent, model 6060). The front PTR configuration was obtained by inserting a mirror (Mirror 1 in Fig. 3), allowing the laser beam to impinge on the metallic sample surface facing the off-axis paraboloidal reflector. The rear PTR configuration was obtained by removing mirror 1
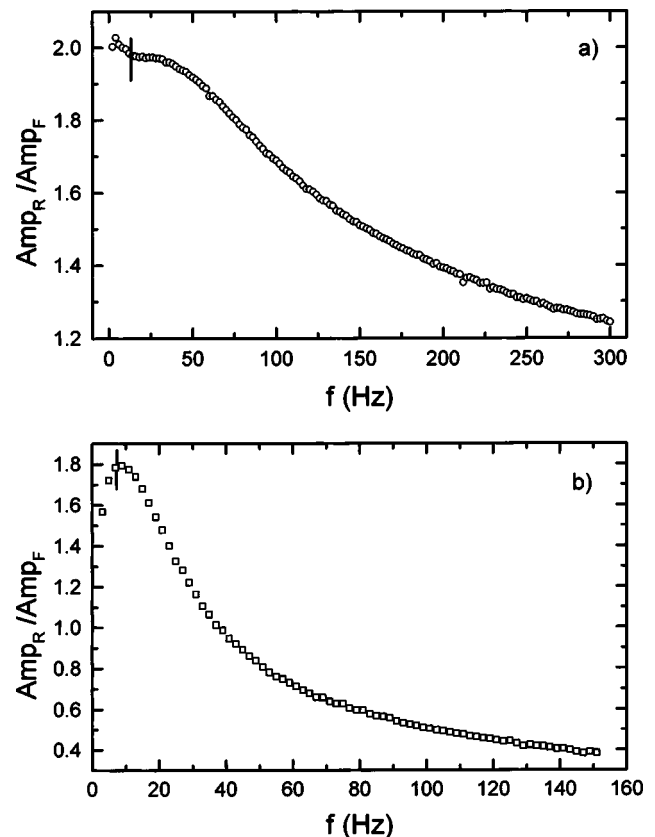

FIG. 4. Ratio of amplitudes for the rear and front PA configurations, as a function of modulation frequency. (a) Aluminum, thickness 300 μm. (b) Steel, thickness 560 μm.
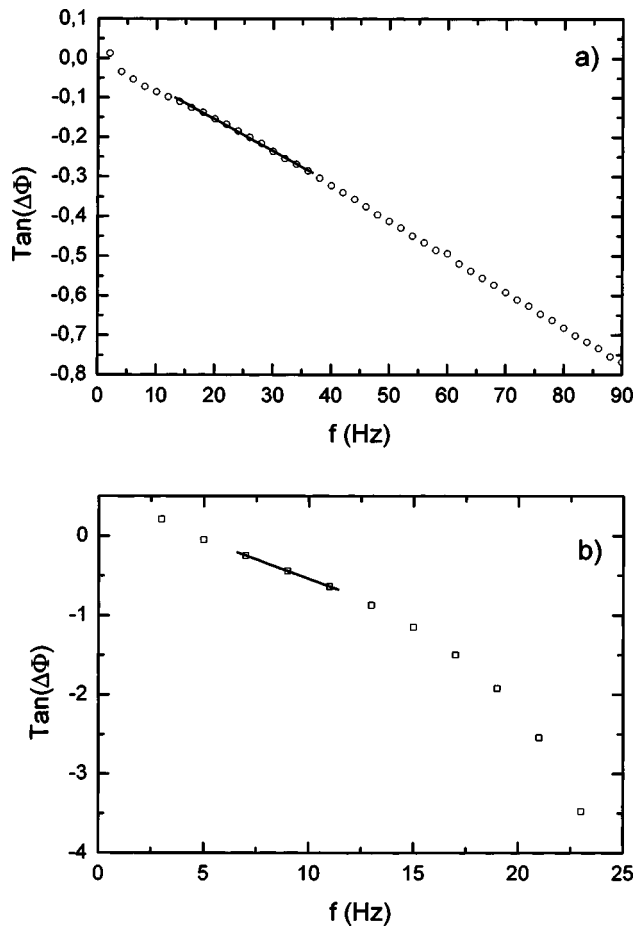
FIG. 5. Tangent of phase difference between rear and front PA configurations, as a function of modulation frequency. (a) Aluminum, thickness 300 μm. (b) Steel, thickness 560 μm.

FIG. 6. Phase difference between rear and front PA configurations, as a function of modulation frequency. (a) Aluminum, thickness 300 μm. (b) Steel, thickness 560 μm.

and allowing the laser beam to impinge on the back surface of the sample. The infrared sensor consisted of a HgCdTe photodetector element, 1 mm^2 of active area (Judson Technologies, J15 Series).

IV. EXPERIMENTAL RESULTS

Figure 4 shows the ratio of PA amplitudes for the aluminum and steel samples. The vertical lines in Fig. 4 identify the regions below which 3D effects appear through deviations from the linear behavior predicted by Eq. (5) in the low-f limit. Alternatively, a possibility exists that the air column inside the PA cell is thermally thin. To avoid these possible complications, the analysis using the PA signal ratio for our materials was limited in the frequency range above 13 Hz for the aluminum sample and 7 Hz for the steel sample. The self-normalized phase, $\Delta\Phi$, results are shown in Fig. 5(a) for aluminum and Fig. 5(b) for steel, where Eq. (7) was fitted to the data. The continuous lines are the best fits of the 1D Eq. (7) in this frequency range. The thermal diffusivity values obtained through best fits to the PA data and are summarized in Table I, column 3. Deviations from the linear behavior with f predicted for the tangent of phase difference in Eq. (7) are evident above 37 Hz for the aluminum sample [Fig. 5(a)], and above 11 Hz for the steel sample [Fig. 5(b)]. Therefore, the linear analysis was not used above these
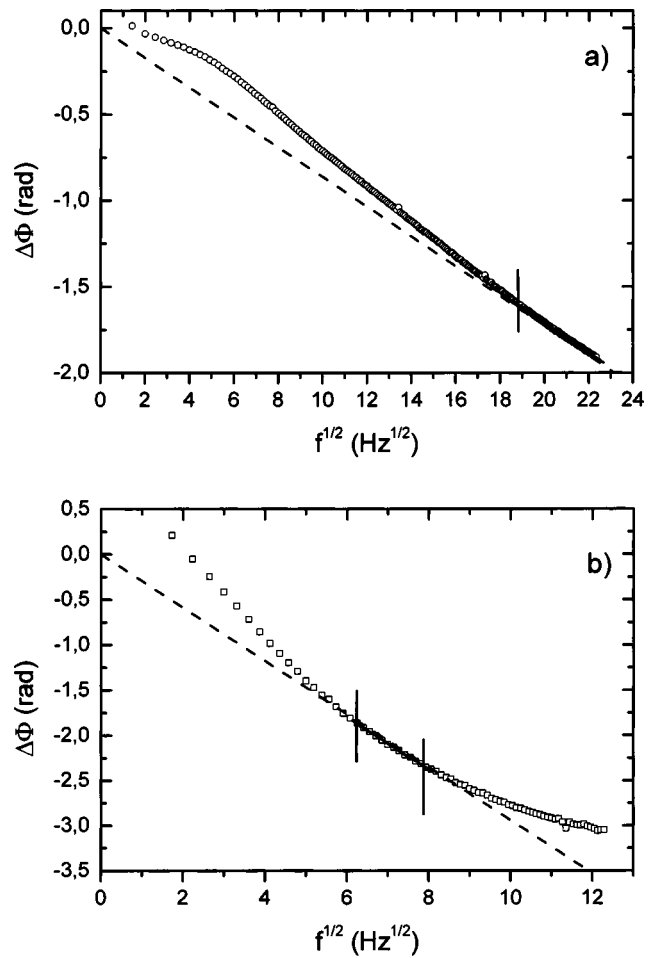
boundary frequencies for the aluminum and steel thin samples, respectively. The corresponding plots involving the thermally thick ranges are shown in Fig. 6. The dashed lines in Fig. 6 were used to identify the modulation frequency ranges where the PA signal is dominated purely by thermal waves with negligible contributions from thermoelastic effects. These lines were drawn following the criterion that $\Delta\Phi$ must cross the origin as the modulation frequency approaches zero, as predicted in Eq. (6). The application of this criterion for quantitative photothermal measurements is essential, especially in the steel sample case shown in Fig. 6(b), where a strong thermoelastic contribution is evident at low frequencies as expected from the small thickness of this sample.[12] The vertical lines on the corresponding plots show the limits (lower limit for the case of the aluminum sample) on modulation frequencies between which experimental data ratios were considered for analysis using Eq. (8). The continuous lines in Fig. 8 are the best fits to this equation and the corresponding values of the measured thermal diffusivity are summarized in Table I, column 4.

Figure 7 shows the ratio of PTR amplitudes for the two samples. The poor signal-to-noise ratio (SNR) for the aluminum sample is evident, and is in contrast with the corresponding PTR ratio for the steel sample. The poor aluminum SNR is due to the high reflectivity and low infrared emissiv-
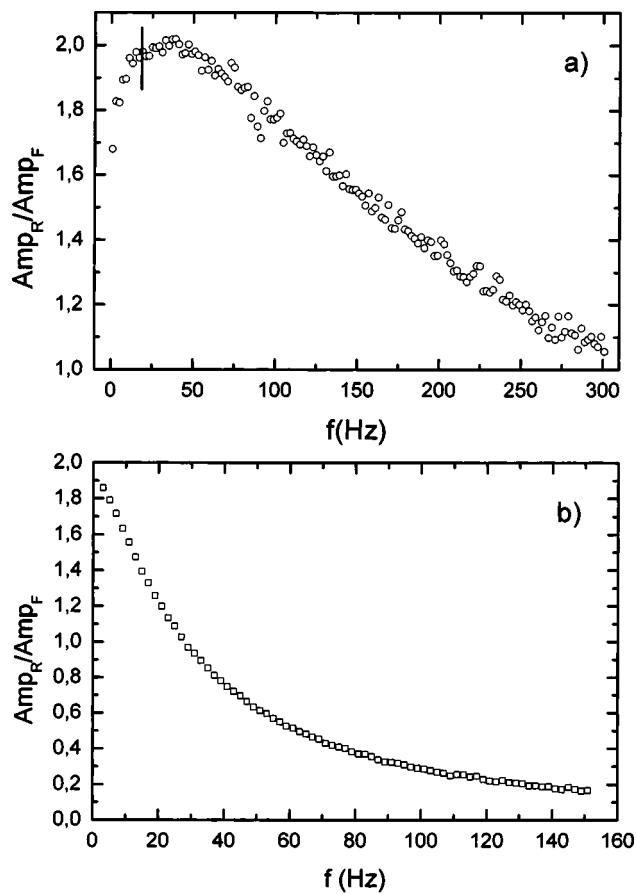
FIG. 7. Ratio of amplitudes for the rear and front PTR configurations, as a function of modulation frequency. (a) Aluminum, thickness 300 μm. (b) Steel, thickness 560 μm.
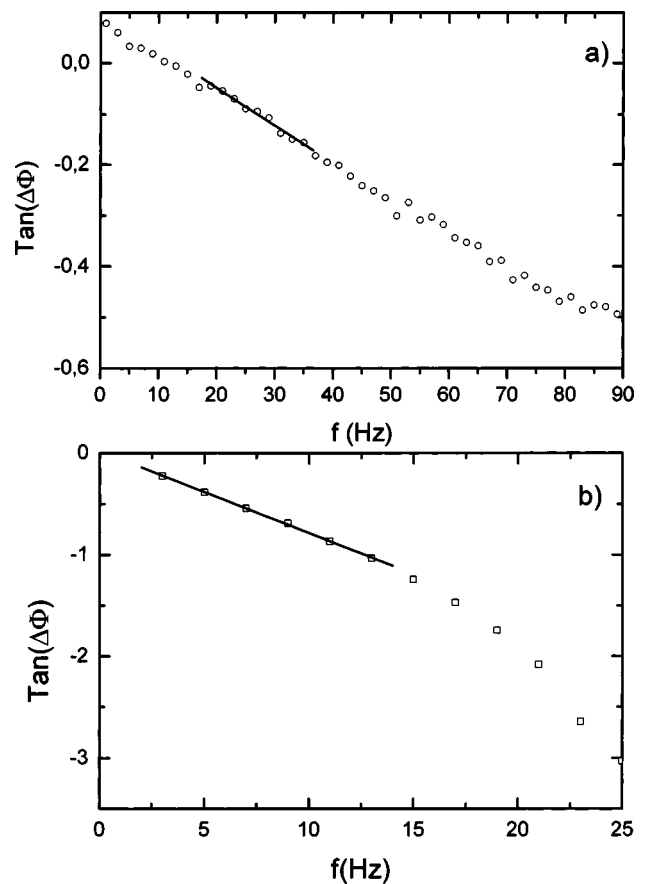

FIG. 8. Tangent of phase difference between rear and front PTR configurations, as a function of modulation frequency. (a) Aluminum, thickness 300 μm. (b) Steel, thickness 560 μm.

ity of the aluminum sample as well as its high thermal conductivity which decreases the magnitude of the thermal wave signal at the surface. Another aspect worth noting is the absence of 3D effects for the steel sample at very low modulation frequencies. To avoid 3D effects in the 1D measurements of the aluminum sample, the analysis of the PTR phase differences was carried above 19 Hz, as suggested by the amplitude ratios in Fig. 7(a). Figure 8 shows the range of modulation frequencies where the fit of the PTR data to Eq. (7) was carried out. The continuous lines in Fig. 8 are the best fits of this equation in the selected frequency ranges. The thermal diffusivity values were obtained following the same procedure as described for the PA results and are summarized in Table I, column 5. The corresponding results at high frequencies are shown in Fig. 9. The same procedure as with the PA data was followed, with the simplification that PTR signals are generated through radiation emission only and they are insensitive to synchronous thermoelastic vibrations in the metal. The effects of thermoelastic contributions to the PA phase are very easily seen upon comparison of Figs. 6(b) and 9(b). The continuous lines in Fig. 9 are best fits of Eq. (8) to the PTR $\Delta\Phi$ data. The extracted values of the thermal diffusivity are summarized in Table I, column 6.

V. DISCUSSION

Table I shows that the self-normalized PA measurements using the thermally thin and thick frequency responses from the two metal samples yield very consistent thermal diffusivity results for both samples used in this work. The literature values for bulk aluminum metal are in the 0.8–0.98 cm²/s range,[13] however, it is expected[14] that very thin layers of aluminum will have lower thermal diffusivity values, as measured in this work. The decrease in the thermal diffusivity of thin layers compared to bulk materials is due to the poorer quality of imperfectly grown or manufactured/machined thin layers. With regard to steels, the thermal diffusivity value depends on the composition of a particular steel. The reported values[15,16] in the range 0.037–0.14 cm²/s are somewhat higher than the measured values in Table I, again, as expected from thin steels. PTR produced diffusivity values very consistent with the PA results only in the case of the steel sample. The higher value obtained from the thermally thick aluminum measurement may be due to the well known large thermal expansion coefficient of this metal, which was not taken into account in the theoretical interpretation. Laser induced thermomechanical expansion is known to generate PTR signals in aluminum through surface motion which tends to affect the high-frequency signal and yield overestimates in the value of the thermal diffusivity of aluminum, unless accounted for theoretically.[17]

In conclusion, a general PT self-normalized scheme has been developed for thermal diffusivity measurements of thin metallic layers. Two independent but complementary photothermal techniques were used to validate the scheme: PT
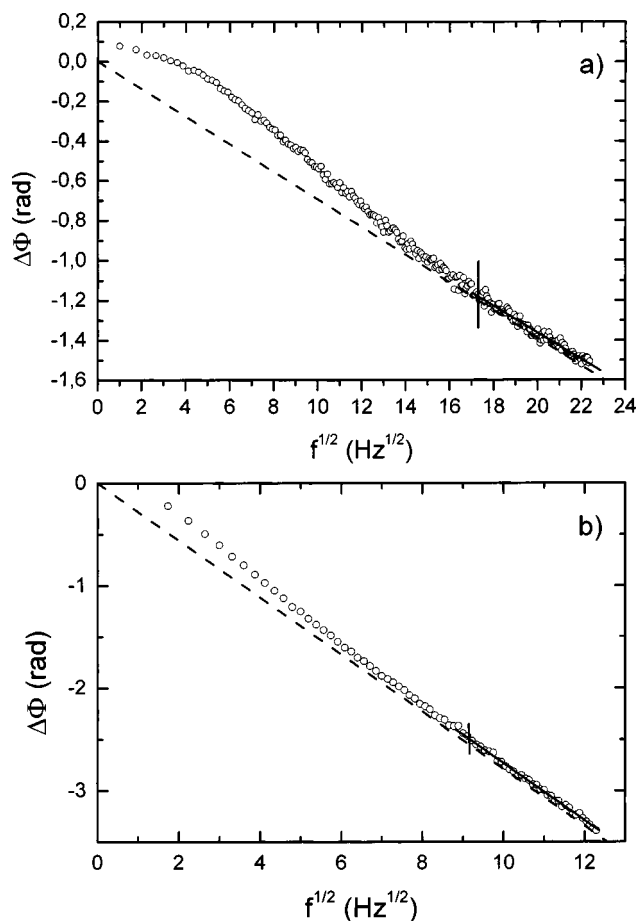
FIG. 9. Phase difference between rear and front PA configurations, as a function of modulation frequency. (a) Aluminum, thickness 300 μm. (b) Steel, thickness 560 μm.

radiometry and gas-cell PA detection. The corresponding measurement procedures involve linear fits in the photothermally thin and/or thick limits. Experimental criteria have been developed to ascertain that a purely thermal-diffusion-wave mechanism is dominant throughout the selected frequency range, thus validating the accuracy of the thermal

diffusivity measurements. These aspects represent advantages in terms of simplicity and reliability over earlier similar self-normalized schemes which use exact PT formulations but no proper, easy to check, criteria to assure their validity frequency ranges, especially in the light of competing nondiffusion-wave mechanisms.[3,7] Experiments with thin layers of aluminum and steel yielded self-consistent values between thermally thin and thick measurements. The PTR technique has the advantage of insensitivity to thermoelastic contributions to the signal, but exhibits additional contributions from the thermal expansion mechanism in aluminum.

ACKNOWLEDGMENT

[1] A. Mandelis, S. B. Peralta, and J. Thoen, J. Appl. Phys. **70**, 1761 (1991).
[2] G. Rousset and F. Lepoutre, J. Appl. Phys. **54**, 2383 (1983).
[3] L. F. Perondi and L. C. M. Miranda, J. Appl. Phys. **62**, 2955 (1987).
[4] J. A. Balderas-López, J. M. Náñez-Limón, S. A. Tomás, H. Vargas, V. Olalde-Portugal, R. Baquero, I. Delgadillo, and L. C. M. Miranda, Forest. Prod. J. **46**, 84 (1986).
[5] J. A. Balderas-López and A. Mandelis, J. Appl. Phys. **12**, 2045 (2000).
[6] J. A. Balderas-López and A. Mandelis, J. Appl. Phys. **90**, 2273 (2001).
[7] O. Pessoa, Jr., C. L. Cesar, N. A. Patel, H. Vargas, C. C. Ghizoni, and L. C. M. Miranda, J. Appl. Phys. **59**, 1316 (1986).
[8] A. Roscenwaig and A. Gersho, J. Appl. Phys. **47**, 64 (1976).
[9] R. Santos and L. Miranda, J. Appl. Phys. **52**, 4194 (1981).
[10] A. Mandelis, *Diffusion-Wave Fields: Mathematical Methods and Green Functions* (Springer, New York, 2001), Chap. 2.
[11] *Mathematical Handbook*, edited by M. R. Spiegel (Schaum's Outlines. 35th Printing) (McGraw–Hill, New York, 1996).
[12] G. Rousset, P. Cielo, and L. Bertrand, J. Appl. Phys. **57**, 4396 (1985).
[13] R. L. Thomas, L. D. Favro, D. S. Kin, P. K. Kuo, C. B. Rayes, and S. Y. Zhang, Rev. Prog. Quant. Nondestr. Eval. **6**, 271 (1990).
[14] O. W. Kading, H. Skurk, and E. Matthias, J. Phys. (Paris) **4**, C7-619 (1994).
[15] A. Rosencwaig, in *Advances in Electronics and Electron Physics*, edited by L. Marton (Academic, New York, 1978), Vol. 46, p. 207.
[16] W. L. Parker, R. J. Jenkins, C. P. Butler, and G. L. Abbott, J. Appl. Phys. **32**, 1679 (1961).
[17] M. Munidasa, A. Mandelis, and M. Ball, Rev. Sci. Instrum. **69**, 507 (1998).